

# HCN4 channels sense temperature and determine heart rate responses to heat

Received: 19 March 2024

Accepted: 18 February 2025

Published online: 01 March 2025



Yuejin Wu<sup>1,6</sup>✉, Qinchuan Wang<sup>1,6</sup>, Jonathan Granger<sup>1</sup>,  
Oscar Reyes Gaido<sup>1</sup>, Gabriel Lopez-Cecetaite<sup>1</sup>, Eric Nunez Aguilar<sup>2</sup>,  
Andreas Ludwig<sup>3</sup>, Anna Moroni<sup>4</sup>, Mario A. Bianchet<sup>2</sup> &  
Mark E. Anderson<sup>1,5</sup>✉

The hyperpolarization-activated cyclic nucleotide-gated ion channel 4 (HCN4) current increases due to cAMP binding and is well-recognized to contribute to adrenergically driven heart rate acceleration. HCN4 current also increases with heat by an unknown mechanism(s). We use thermodynamical and homology computational modeling, site-directed mutagenesis, and mouse models to identify a concise motif on the S4-S5 linker of HCN4 channels (M407/Y409) that determines HCN4 current ( $I_f$ ) responses to heat. This motif is required for heat-triggered rate acceleration in cardiac pacemaker cells, isolated hearts and in vivo. Surprisingly, a loss of function M407/Y409 motif mutation prevented not only normal heat but also cAMP responses, suggesting that the heat-sensing machinery within the S4-S5 linker is essential for operating the cAMP allosteric pathway and is central to HCN4 gating modulation. The M407/Y409 motif is conserved across all HCN family members suggesting that HCN channels participate broadly in coupling heat to changes in cell membrane excitability.

Heart rate increases with heat<sup>1–3</sup>, constituting a fundamental physiological relationship in vertebrates. HCN channels (HCN1–4) govern cell membrane excitability in neurons, smooth muscle, and heart. All HCN family members are activated by hyperpolarization and equipped with a cyclic nucleotide-binding domain<sup>4</sup>. HCN4, the predominant HCN channel expressed in cardiac sinoatrial nodal (SAN) pacemaker cells, initiates each normal heartbeat by a cell membrane depolarizing inward current ( $I_f$ )<sup>5</sup> that triggers an action potential. The SAN cell  $I_f$  is augmented in response to extracellular catecholamines by an adrenergic receptor-mediated increase in cyclic adenosine monophosphate (cAMP), an intracellular second messenger that binds to HCN4 cyclic nucleotide binding domain. cAMP binding increases  $I_f$  to accelerate SAN action potentials and heart rate, as part of a physiological

‘fight or flight’ response.  $I_f$  increases with heat with a temperature coefficient ( $Q_{10}$ ) of ~ 2<sup>6,7</sup> but the mechanisms for coupling thermal energy to HCN4 are unknown and the role of HCN4 in heart rate responses to heat is unexplored.

Heart rates are increased by heat in humans and in mice, with a  $Q_{10}$  ~ 2<sup>2,8</sup>, constituting a conserved stress response operated by an unknown mechanism<sup>9</sup>. Understanding the interrelationship between heat, cell membrane excitability and heart rate is an important goal for the life sciences<sup>10</sup>, in part, because of rising temperatures worldwide<sup>11,12</sup>. A recent meta-analysis reported that a temperature increase of just 1 °C is associated with a 2.1% increase in the risk of death related to cardiovascular disease<sup>10</sup>. Given the central role of HCN4 in heart rate acceleration and the

<sup>1</sup>Department of Medicine, Johns Hopkins School of Medicine, Baltimore, MD, USA. <sup>2</sup>Department of Biophysics and Biophysical Chemistry, Johns Hopkins University School of Medicine, Baltimore, MD, USA. <sup>3</sup>Institut für Experimentelle und Klinische Pharmakologie und Toxikologie, Friedrich-Alexander-Universität Erlangen-Nürnberg, Erlangen, Germany. <sup>4</sup>Department of Biosciences, University of Milan, via Celoria 26, 20133 Milan, Italy. <sup>5</sup>Department of Medicine and Division of Biological Sciences, University of Chicago, Chicago, IL, USA. <sup>6</sup>These authors contributed equally: Yuejin Wu, Qinchuan Wang.

✉ e-mail: [ywu95@jhmi.edu](mailto:ywu95@jhmi.edu); [andersonm1@uchicago.edu](mailto:andersonm1@uchicago.edu)

known temperature dependency of  $I_f$  in SAN<sup>6</sup> and Purkinje fibers<sup>7</sup>, we asked if HCN4 contributed to heart rate responses to heat.

Here, we show that HCN4 responds to temperature with a  $Q_{10}$  of ~2, resembling the native  $I_f$  current. We identify a heat-resistant mutant (M407Q/Y409F) of the HCN4 channel whose current lacks augmentation by heat and is unresponsive to cAMP. In contrast, a mutant HCN4 channel lacking a functional cAMP binding domain<sup>13</sup> but retaining the M407/Y409 motif maintains responsiveness to heat. Using mouse SAN cell models and CRISPR/Cas9-generated mice harboring the M407Q/Y409F mutation, we demonstrate that the M407/Y409 motif is critical for heat sensing and physiological coupling of HCN4 to heart rate increases in response to heat. We further show that the M407/Y409 motif is required for heat sensing in HCN1, 2, and 4. Our findings reveal primacy of heat sensing in enabling cAMP-dependent activation of HCN channels and suggest that HCN channels participate broadly in thermal contributions to cell membrane excitability.

## Results

### Heat-induced rate increases in cardiac pacemaker cells require HCN4 and $I_f$

Because the basis for heat induced heart rate increases is unknown, we first asked if spontaneous action potential rates in current clamped isolated SAN cells (Fig. 1a) are thermally responsive. The action potential rates recorded from single SAN cells increased with increased temperatures in the range of 30–44 °C (Supplementary Fig. 1a). Because the Arrhenius plots from those data all show a linear dependency on temperature (Supplementary Fig. 1b), we quantified SAN responses to heat using an established temperature coefficient,  $Q_{10}$  ( $Q_{10} = (R_2/R_1)^{10/(T_2-T_1)}$ ) where  $R$  is the rate of spontaneous action potentials measured at a given temperature,  $T$ .  $Q_{10}$  reported in our studies is calculated by paired  $R_2$ ,  $R_1$  and  $T_2$ ,  $T_1$  from the same experimental sample, be it an isolated cell, heart or mouse (see Methods). In vertebrates the  $Q_{10}$  for heart rate in vivo is ~2.0<sup>14</sup>, equivalent to doubling of heart rate over a 10 °C temperature range.

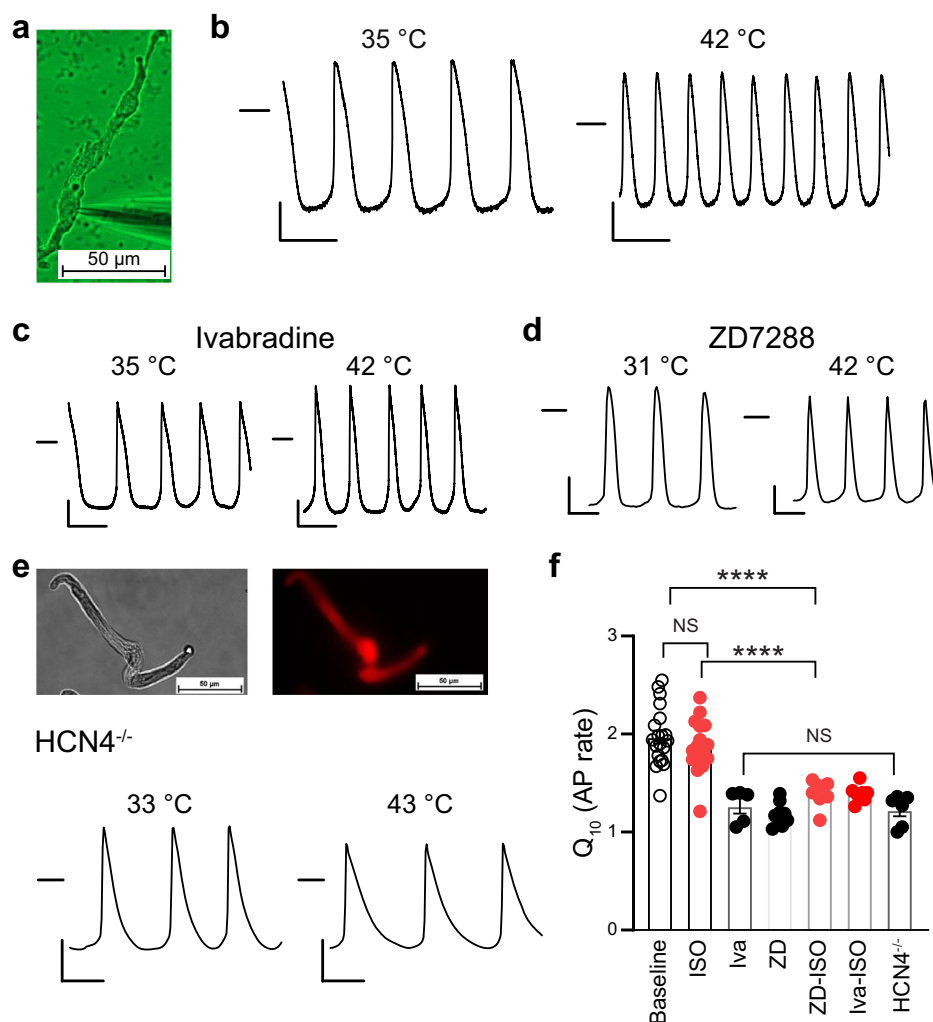


**Fig. 1 | HCN4 antagonists or *Hcn4* knock out prevent action potential rate increases by heat in SAN cells.** **a** Isolated SAN cell in whole cell mode current clamp configuration, scale bar = 50  $\mu$ m. **b** Representative SAN cell action potential (AP) tracings recorded under lower (left) and increased temperature (right) from the same SAN cell. **c** Representative SAN cell AP tracings recorded in the presence of HCN4 antagonist agents Ivabradine (4  $\mu$ M) or (d) ZD7288 (4  $\mu$ M) under lower (left) and increased temperature (right). The AP was recorded at different temperatures but from the same SAN cell in each case. **e** upper panel, Example of adenovirus-infected SAN cells from floxed mice expressing mCherry and Cre (red, right) (scale bar = 50  $\mu$ m). lower panel, Representative AP tracings recorded under

lower basal (left) and increased temperature (right) conditions from the same cultured single SAN cells isolated from *Hcn4*<sup>flx/flx</sup> mice cultured in the presence of adenovirus expressing Cre recombinase (see Methods). **b–e** the horizontal lines mark 0 mV. Scale bars are 200 ms horizontal and 20 mV vertical. **f** Summary data for  $Q_{10}$  from SAN cell AP rate responses to temperature increases. The presence of isoproterenol (ISO, 1  $\mu$ M), Ivabradine (Iva, 4  $\mu$ M), or ZD7288 (ZD, 4  $\mu$ M) in the bath solution is indicated. Data are presented as mean values  $\pm$  SEM. One-way ANOVA, \*\*\* $p$  < 0.001, \*\*\*\* $p$  < 0.0001,  $p$  (baseline vs. ISO) 0.8,  $p$ -values for comparisons of right 5 groups are from 0.52 > 1. ( $n$  = 20 Baseline,  $n$  = 17 ISO,  $n$  = 5 Iva,  $n$  = 9 ZD,  $n$  = 7 ZD-ISO,  $n$  = 8 Iva-ISO,  $n$  = 6 HCN4<sup>-/-</sup>).

We found that spontaneous action potential rates increase with rising temperature in SAN cells isolated from mice (Fig. 1b). They have a  $Q_{10}$  of  $1.97 \pm 0.07$  ( $n = 20$ , Fig. 1), similar to heart rate responses to heat in vivo, in humans and other vertebrates<sup>8,14–16</sup>.

Two  $I_f$  antagonist drugs (ivabradine<sup>17</sup> and ZD7288<sup>18</sup>) prevented SAN thermal rate responses ( $Q_{10} = 1.27 \pm 0.08$  ( $n = 5$ ) for ivabradine and  $1.18 \pm 0.04$  ( $n = 9$ ) for ZD7282,  $p < 0.001$  as compared to control condition, Fig. 1c, d), without affecting rate increases from isoproterenol (Supplementary Fig. 2a), a  $\beta$ -adrenergic receptor agonist that accelerates heart rate by HCN4 and cAMP dependent and independent pathways<sup>19</sup>. We cultured SAN cells isolated from mice where *Hcn4* was flanked by LoxP insertions (*Hcn4*<sup>L2/L2</sup>)<sup>20</sup>. These SAN cells were infected with adenovirus expressing Cre recombinase and a red fluorescent protein marker (mCherry, see Methods, Fig. 1e) for 24 h to generate *Hcn4* knock out (*Hcn4*<sup>-/-</sup>) SAN cells. These *Hcn4*<sup>-/-</sup> SAN cells, identified by the presence of mCherry, lacked HCN4 current,  $I_f$  (Supplementary Fig. 2b), indicating successful excision of *Hcn4* by Cre recombinase. Consistent with our findings using  $I_f$  antagonist drugs, cultured *Hcn4*<sup>-/-</sup> SAN cells lacked thermal responses ( $Q_{10} = 1.23 \pm 0.06$  ( $n = 6$ ), Fig. 1e).

In addition to  $I_f$ , Calcium/Calmodulin-dependent kinase II (CaMKII) activation<sup>19</sup> contributes to SAN cell rate increases during adrenergic stress and is potentially sensitive to temperature. SAN cells with CaMKII inhibition due to transgenic expression of an inhibitory peptide, AC3-I, have diminished rate responses to isoproterenol<sup>19</sup>. However, we found that AC3-I expressing SAN cells showed similar rate increases in response to temperature compared to SAN cells isolated from WT littermates (Supplementary Fig. 2c). Taken together (Fig. 1f), these findings supported a concept that SAN cell action potential rates were increased by thermal energy, similar to in vivo heart rate responses, and suggested that  $I_f$  was responsible for all or most of SAN cell heat sensitivity.

### **$I_f$ has a $Q_{10}$ that is independent of cAMP signaling**

Given our findings showing HCN4 and  $I_f$  were essential for heat mediated SAN cell action potential frequency increases, we next performed voltage clamp experiments on isolated SAN cells and found  $I_f$  was enhanced by increasing temperatures between 28 °C–45 °C (Fig. 2a and Supplementary Fig. 3). The  $Q_{10}$  calculated for the steady state current at cell membrane test potentials from -60 mV – -130 mV was around 2 and showed a slight but statistically significant voltage dependency (e.g.,  $2.15 \pm 0.11$  at -60 mV,  $1.94 \pm 0.30$  at -130 mV,  $n = 11$ ,  $p = 0.026$ ).

In order to determine if the  $I_f$  heat response was related to SAN cell specific elements, we transfected (human) HCN4 cDNA into human embryonic kidney 293 (HEK) cells. The HCN4 channel current recorded from HEK cells increased with heat in the similar manner as in SAN cells (Fig. 2b).

To uncover the mechanism underlying the heat induced increase in current we plotted the tail currents of cells at low and elevated temperatures (Fig. 2c, left panel). Fitting data to a Boltzmann function shows that heat augments the HCN4 current by affecting two components: it increases the amplitude of the steady state current by a factor of 1.6 which can be attributed either to an increase in the unitary conductance or an increase in the number of channels in the plasma membrane. Temperature also seems to affect the open probability causing a positive shift of the activation curve by 10 mV. To quantify this effect more precisely the same data were normalized to values between zero (channel fully closed) and one (maximal open probability) and refitted to the Boltzmann function (Fig. 2c, right panel). This yielded a mean temperature induced shift of the  $V_{1/2}$  value of  $11.3 \pm 1.6$  mV ( $n = 20/21$ ) (Fig. 2c, right panel and Supplementary Table 2). This positive effect of temperature on voltage-dependent activation of  $I_f$  and the HCN4 channel is anticipated by the activation kinetics of the currents that appears faster at higher temperature (e.g., Fig. 2a, b). To quantify this effect, we fitted the rise in HCN4 inward

current in response to a voltage step from -40 mV to -130 mV with a single exponential, at low and high temperatures. The data in Fig. 2d show that heat is indeed accelerating the time constant of channel activation.

The dual effect of temperature on HCN4 current predicts that the impact of heat is stronger at voltages at which the open probability is not yet saturated e.g., voltages below -130 mV. The analysis of  $Q_{10}$  values at -130 mV and -60 mV confirms this prediction. At -130 mV we estimate in the present example (Fig. 2b) a  $Q_{10}$  value of 1.45 (mean  $1.79 \pm 0.11$ ,  $n = 28$ ). The same analysis at -60 mV provides a  $Q_{10}$  value of 1.92 (mean  $2.29 \pm 0.13$ ,  $n = 28$ ,  $p = 0.006$  compared to the  $Q_{10}$  value at -130 mV). Similar to the measurements of  $I_f$  currents in SAN cells, the  $Q_{10}$  value is indeed higher at -60 mV than at extreme negative voltages because at -60 mV heat likely has a dual impact, augmenting gating and conductance.

Our findings underline that the HCN channel is more sensitive to temperature at moderate physiological membrane potentials than at high non-physiological negative voltages. In order to relate the impact of temperatures on channel function to the observed influence on action potential frequency we chose to focus the further analysis on  $Q_{10}$  values at -60 mV, a physiologically relevant cell membrane potential for SAN cells. The  $Q_{10}$  for HCN4 current recorded from HEK cells was similar in the presence or absence of cAMP dialysis (Fig. 2e) while ivabradine and ZD7288 prevented the  $I_f$  response to heat in SAN cells with or without ISO (Fig. 2f). Similar to SAN action potential rates, heat increased HCN4 current, apparently by a mechanism that is independent of cAMP.

### **HCN4 temperature responses rely on a concise intracellular linker motif**

Based on our findings that HCN4 conducts a heat-responsive current, we next sought to identify the mechanism modulating the channel thermal responses. The heat dependence of channel activation is a function of the curvature of free energy ( $\Delta G(T)$ )<sup>21</sup>. Such curvature depends on the variation of the specific heat ( $C_p$ ) at constant pressure  $\Delta C_p(T)$  (see Supplementary material and Eq. 1–6).  $\Delta C_p(T)$  in proteins is mostly a function of the area exposed to the solvent<sup>21</sup> and its variation during channel activation is related to the change in the solvent-accessible surface area (SASA). For instance, an unfolding event is usually characterized by an increase in  $C_p$  due to solvation of hydrophobic residues.

To identify candidate amino acids making significant contributions to the HCN4 temperature response, we used a common-sense approach: focusing our search on residues of protein regions exhibiting significant changes in SASA measured between the two states represented by the structures of the cAMP-free and cAMP-bound (activated) states of the HCN4 channel.

We performed a comparison of the human HCN4 structures extending it to rabbit ortholog HCN4. This analysis helped us to pinpoint by thermodynamic analysis specific residues that modulate HCN4 thermal responses. The HCN4 protein forms a pore as an aggregation of four subunits. Each of the subunits consists of six membrane spanning domains (transmembrane S1–S6) connected by intra- and extracellular linkers. There is a prominent intracellular C terminus that contains the cyclic nucleotide binding domain (CNBD) (Fig. 3a) connected to the S6 via a C-linker that forms the “disk domain” (Fig. 3a). Binding of cAMP to the CNBD induces conformational changes that are transmitted to the transmembrane region via the C-linker and facilitate pore opening. Even though HCN4 channels require hyperpolarizing voltages to move the voltage sensor and to open the pore, the conformational changes induced by cAMP binding in the cytosolic domain are present in the cryoEM structures of the channel solved in the absence of voltage (0 mV). We define this state as “activated” in our analysis below, indicating that the cytosolic machinery is in its signal transmitting configuration. The overlap of

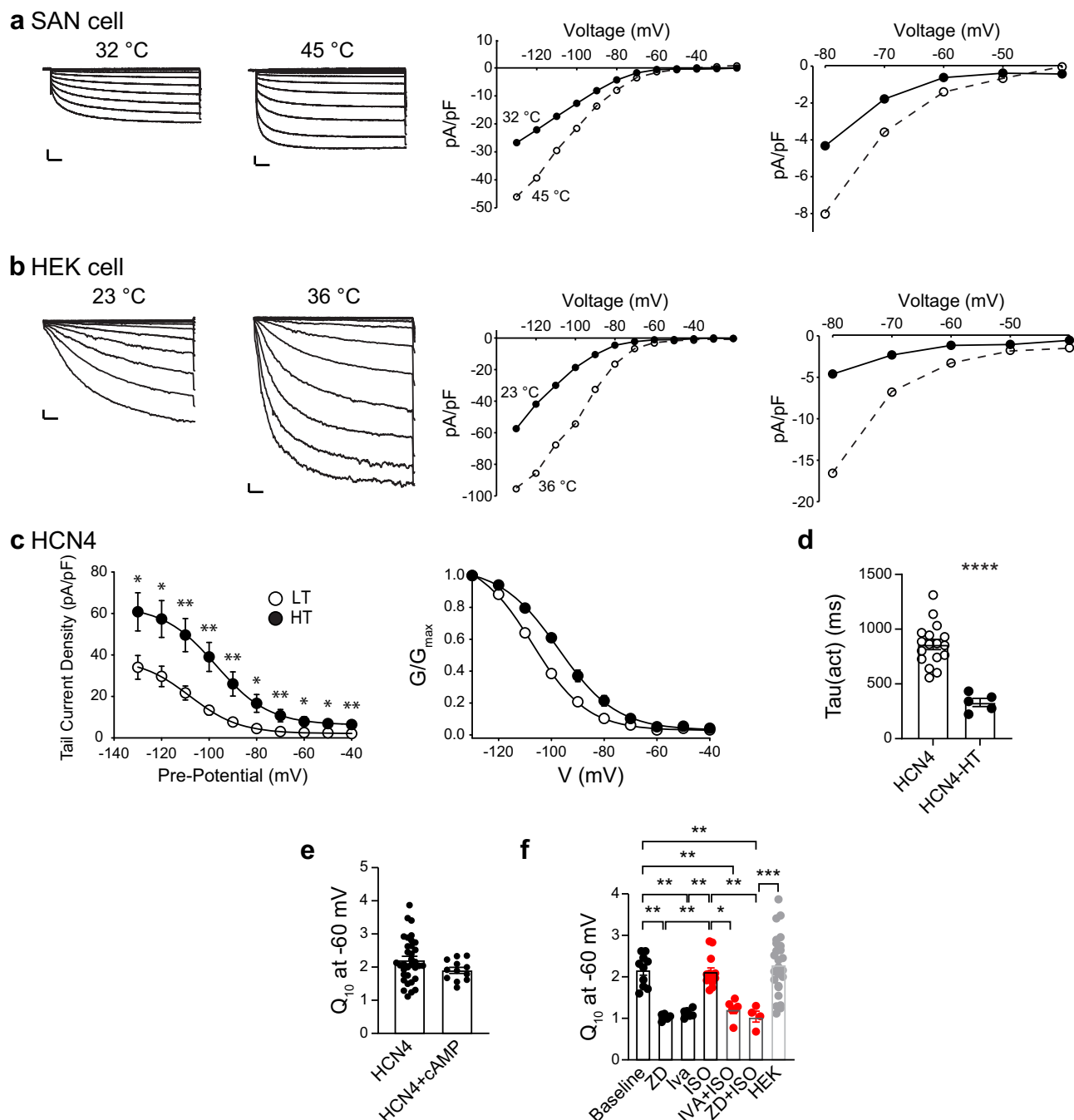
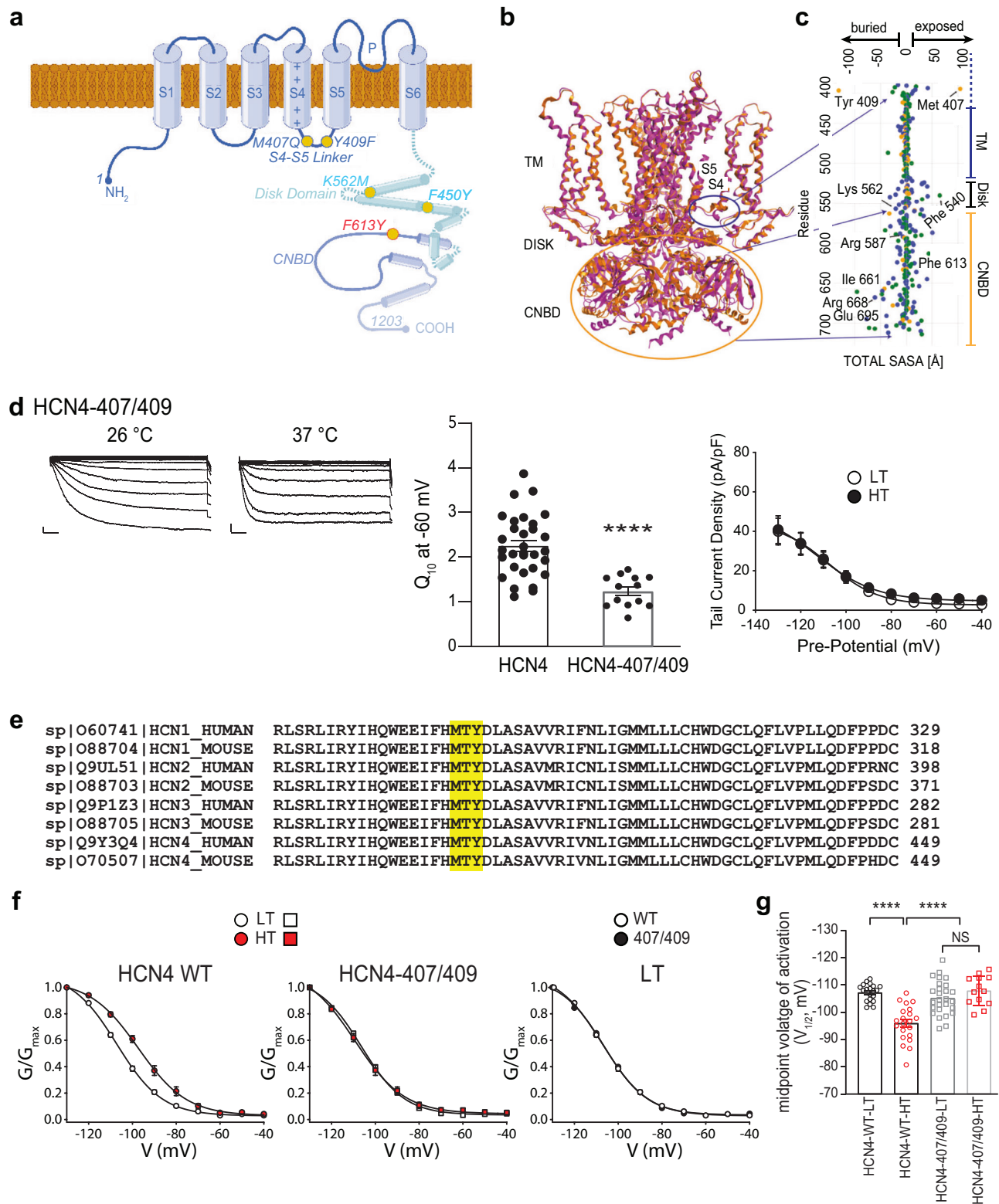


**Fig. 2 | HCN4 current ( $I_h$ ) has a  $Q_{10}$  of ~2.0 that is independent of cAMP signaling.**

Representative  $I_h$  (HCN4 current) tracings recorded under lower and increased temperatures (left panels) from (a), the same isolated SAN cell or (b) in the same human embryonic kidney cell (HEK) transfected with *HCN4* (see Methods). Current-voltage relationship from the same cell (right panels, filled circles lower temperature and open circles higher temperature). The right-most panels expanded to highlight the physiological cell membrane potential range for SAN cells (-40 – -80 mV). The horizontal scale bar is 500 ms and the vertical scale bar is 5 pA/pF in both (a) and (b). **c** Activation curves from absolute (left) or normalized tail current values (right) from HEK 293 cells expressing *HCN4*, before and after temperature increase (empty circle: lower temperature, filled circle: higher temperature). Data are presented as mean values  $\pm$  SEM. Solid lines show Boltzmann fitting to the data (Eq. 1, see Methods) yielding the following values of  $V_{1/2}$ :  $-107 \pm 1$  mV (LT) and  $-97 \pm 2$  mV (HT) in left panel and  $-107 \pm 0.7$  (LT) and  $-96 \pm 1.2$

(HT) in right panel. The  $G_{max}$  values: 35.9 (LT) and 57.3 (HT), and  $A$  values (offset): 2.11 (LT) and 6.42 (HT) in left panel. Student's  $t$ -test or Mann-Whitney Rank Sum Test applied when appropriate, (\* $p < 0.05$ , \*\* $p < 0.01$ , \*\*\* $p < 0.001$ , \*\*\*\* $p < 0.0001$  by Student's  $t$ -test (two-tailed)). **e** Summary data for  $Q_{10}$  from HCN4 channel currents at -60 mV from HEK cells expressing *HCN4* in the presence ( $n = 12$ ) or absence of cAMP ( $n = 34$ ). Data are presented as mean values  $\pm$  SEM. **f** Summary  $Q_{10}$  data for  $I_h$  at -60 mV from isolated SAN cells treated with ISO (1  $\mu$ M,  $n = 13$ ), and/or Ivabradine (Iva, 4  $\mu$ M,  $n = 6$ , Iva+ISO,  $n = 6$ ) or ZD7288 (ZD, 4  $\mu$ M,  $n = 5$ , ZD + ISO  $n = 4$ ),  $n = 10$  Baseline,  $n = 26$ , HEK. Data are presented as mean values  $\pm$  SEM. One-way ANOVA \* $p < 0.05$ , \*\* $p < 0.01$ , \*\*\* $p < 0.001$ .





the human HCN4 structures, the cAMP free (PDB:6GYN) and cAMP-bound (activated) (6GYO) (Fig. 3b) shows that, relative to the other domains, the transmembrane portion of the channel displays significantly less changes than the cytosolic domains. For example, in the human channel the root-mean-square deviation (rmsd), which quantifies the average distance between backbone atoms of the superimposed channel structures, differences between transmembrane domains (a.a. 208–530) of cAMP-free channel shows a rmsd of 1.05 Å<sup>2</sup> for backbone atoms, while the disk (a.a. 521–573) has an rmsd

of 3.55 Å<sup>2</sup> and the cyclic nucleotide binding domain (a.a. 574–718) exhibits an rmsd of 3.94 Å<sup>2</sup>. When the same analysis was repeated by comparing the holo structures of human (6GYO) and rabbit (7NP4) HCN4 structures, minor differences emerged in the S4–5 linker that could affect heat sensing. However, we found that HCN4 channel current heat responses were similar between human (Fig. 2b and e) and rabbit HCN4 expressed in HEK cells (Supplementary Fig. 4a, and Supplemental Notes). Based on this, we focused on human HCN4 for structural and functional studies.

**Fig. 3 | Two amino acids on the 4–5 intracellular linker are essential for heat sensing in HCN4.** **a** Schematic of HCN4 subunit, highlighting the pore, voltage-sensing, intracellular linker, disc, and cyclic nucleotide binding (CNBD) domains. **b** Ribbon diagram showing superimposed HCN4 in apo/closed (6GYN, purple) and holo/activated (cAMP bound, 6GYO, orange) conformations. **c** Total solvent accessible surface area (SASA) exposed or buried in the residues of the S4–5 intracellular linker (top), transmembrane domain (TM), disc, and CNBD in response to channel opening. Apolar (green), polar (blue), and amphipathic (orange) residues are shown. **d** Left, representative HCN4 currents at lower (LT: 24–30 °C) and higher temperatures (HT: 34–43 °C) from cultured HEK 293 cells expressing heat-insensitive HCN4 (M407Q/Y409F). Scale bars: 500 ms (horizontal), 5 pA/pF (vertical). Middle, summary  $Q_{10}$  data for wild type ( $n = 31$ ) and M407Q/Y409F ( $n = 13$ ) HCN4. Data are mean values  $\pm$  SEM. Unpaired Student's  $t$ -test (two-tailed), \*\*\*\* $p < 0.0001$ . Right, mean activation curves (from absolute tail current values) from HEK 293 cells expressing M407Q/Y409F HCN4 channels,

before (LT) and after temperature increase (HT). Data are mean values  $\pm$  SEM. Solid lines show Boltzmann fitting (Eq. 1, see Methods).  $V_{1/2}$  of LT or HT curves:  $-107 \pm 0.7$  mV or  $-113 \pm 1.5$  mV. The  $G_{\max}$  values of LT or HT curves: 41.5 or 45.9.  $n = 13$  for LT or HT groups. **e** Sequence alignment of the 4–5 intracellular linker of human and mouse HCN1–4. **f** Mean activation curves from normalized tail currents of WT (left,  $n = 20$  LT,  $n = 21$  HT) and mutant 407/409 (center,  $n = 27$  LT,  $n = 13$  HT) HCN4 in HEK 293 cells, at low (LT) and high temperature (HT) (WT data are the same as in Fig. 2c). Data are presented as mean values  $\pm$  SEM. Solid lines show Boltzmann fitting (values in Supplementary Table 2). Right panel, data at LT for WT and HCN4<sup>M407Q/Y409F</sup> mutant are replotted for comparison. **g** Summary data (mean values  $\pm$  SEM) for midpoint voltage of activation ( $V_{1/2}$ ). One-way ANOVA with Tukey's multiple comparisons test, \*\*\*\* $p < 0.0001$ ,  $p$ -value for NS is 0.49.  $n = 20$ , HCN4-WT-LT,  $n = 21$ , HCN4-WT-HT,  $n = 27$ , HCN4-407/409-LT,  $n = 13$ , HCN4-407/409-HT. See Supplementary Table 2 for values. Created in BioRender. Aguilar, E. (2025) <https://BioRender.com/o33f198>.

Figure 3c shows the average change in SASA ( $\Delta$ SASA) of the whole human HCN4 channel during channel activation by cAMP. The average value is  $1.3 \text{ \AA}^2$  with a standard deviation ( $\sigma$ (SASA)) of  $16.0 \text{ \AA}^2$ . We analyzed residues showing absolute values of  $\Delta$ SASA  $> 3$  times  $\sigma$ (SASA) ( $> 48 \text{ \AA}^2$ ) between apo and holo (activated) states of the human channel (Supplementary Table 1). The residues with the most significant increases in the apolar area exposed during its activation are Met 407 ( $104 \text{ \AA}^2$ ), Phe 540 ( $54.9 \text{ \AA}^2$ ), and Phe 613 ( $44.4 \text{ \AA}^2$ ), and the most significant decreases, due to polar area sequestration, are Tyr 409 ( $-141.6 \text{ \AA}^2$ ), Arg 668 ( $-57.8 \text{ \AA}^2$ ), and Glu 695 ( $-77.8 \text{ \AA}^2$ ). The hydration of polar and apolar areas of these residues have opposing contributions to the energetics and, as a consequence, to the temperature dependence of processes in which conformational changes are involved.

Met 407 and Tyr 409 are part of the S4–S5 intracellular linker that exhibits a large conformational change after activation (Fig. 3b, c, and Supplementary Movie 1). We excluded residues in disordered regions (e.g., at the C-terminus of the cyclic nucleotide binding domain) from the analysis, focusing on those observed in the structures. To avoid making mutations affecting the activation mechanism, we did not consider residues coordinating intracellular  $\text{Mg}^{2+}$  (His 406, Asp 410, Glu 556 and His 552, Supplementary Fig. 4b)<sup>22</sup>, nor those participating in cAMP binding, such as Ile 661 or Arg 587, and ignored amino acids forming salt bridges stabilizing one particular state of the channel, such as Arg 668 and Glu 695. The above considerations led to a final list of five candidates with the potential to modify the temperature dependence of  $I_f$ : Met 407, Tyr 409, Phe 540, Lys 562, and Phe 613 (see Supplementary Notes). Based on our structural analysis and modeling, and the predicted energy contributions due to its solvation or lack thereof between the closed and cAMP-active HCN4, we designed a set of mutations M407Q, Y409F, F540Y, K562M, and F613Y chosen to minimize residue size variations to limit the structural changes in the mutated protein (see Supplementary Notes). These mutations are predicted to reduce the activation energy barrier or produce positive contributions to the overall  $\Delta\Delta C_p^{\text{mut-wt}}$ , thereby reducing its temperature dependence (lowering  $Q_{10}^{\text{mut}}/Q_{10}^{\text{WT}}$ , equation 5, (see Supplementary Notes). Consistent with our predictions, HCN4 channel current recorded from the 5x mutant HCN4 channel was not responsive to temperature between 27–38 °C (Supplementary Fig. 4c, d).

We next performed a series of studies to evaluate the thermal responsiveness of HCN4 mutants in isolation and various combinations (Supplementary Fig. 4e). These studies revealed M407/Y409 as necessary for conferring thermal responsiveness to HCN4 current (Fig. 3d). This mutant is insensitive to heat and shows no increase in the maximal current nor a shift of the activation curve in response to heat; as a consequence, the  $Q_{10}$  value at  $-60$  mV is close to 1 (Fig. 3d).

Intriguingly, a region of the S4–S5 intracellular linker domain, containing the M407/Y409 residues, was recently identified as important for establishing the melting point for HCN4 protein<sup>22</sup>. This

region includes H406 and D410 that are involved in complexing  $\text{Mg}^{2+}$  together with residues from the C linker domain. These contacts are not present in HCN1(SU6P), and are important in transmitting the cAMP effect in HCN4<sup>22</sup>. Because of the potential role of the S4–5 linker in modulating  $I_f$  through  $\text{Mg}^{2+}$  binding, we dialyzed HEK cells expressing HCN4 with EDTA (10 mM) to chelate  $\text{Mg}^{2+}$ , but failed to detect a change in the temperature response (Supplementary Fig. 4f), supporting our modeling predictions that the role of the S4–5 linker in thermal sensing was independent of its role in  $\text{Mg}^{2+}$  binding. Importantly, M407/Y409 homologous residues, present in the S4–5 intracellular linker domain, are conserved between mice and humans and are present in all HCN family members (Fig. 3e). Currents recorded from HEK cells expressing HCN1 ( $Q_{10} = 2.25 \pm 0.22$ ,  $n = 15$ ) and HCN2 ( $Q_{10} = 2.01 \pm 0.14$ ,  $n = 15$ ) showed similar thermal responses compared to HCN4 (Supplementary Fig. 5a). Consistent with previous studies<sup>23,24</sup>, we were unable to efficiently express HCN3 in HEK cell. Mutation of M407/Y409 homologs in human HCN1 (M287/Y289,  $Q_{10} = 1.10 \pm 0.04$ ,  $n = 18$ ) and HCN2 (M356/Y358,  $Q_{10} = 1.02 \pm 0.05$ ,  $n = 14$ ) eliminated the thermal responses (Supplementary Fig. 5a), demonstrating the general nature of this thermal sensing motif in HCN family channels. We found that temperature increases shifted the half maximal activation voltage ( $V_{1/2}$ , mV) in a depolarized direction for WT HCN4 expressed in HEK 293 cells (Fig. 2c and Supplementary Table 2) and this action was prevented in the temperature insensitive HCN4 M407Q/Y409F mutant (Fig. 3f and Supplementary Table 2). Notably, the M407Q/Y409F mutant showed the same  $V_{1/2}$  of the WT at low temperatures (Fig. 3f, g and Supplementary Table 2), indicating that the mutations do not affect the voltage-gating mechanism of the channel. We found that homologous rabbit HCN4 mutants (M408Q/Y410F) were similarly unresponsive to heat compared to WT (Supplementary Fig. 5b, Supplementary Fig. 4a and Fig. 3d). Taken together, these computational and electrophysiological findings showed that M407/Y409, a component of the intracellular S4–S5 HCN4 linker, is sufficient to account for  $I_f$  increases in response to heat.

### Defective heat-heart rate coupling in M407Q/Y409F Hcn4 knockin mice

We asked if M407/Y409 contributed to heart rate responses to heat. We used CRISPR/Cas9 gene editing to engineer mice with *Hcn4* harboring the M407Q/Y409F mutations (Supplementary Fig. 6). No homozygous knockin mice were born from *Hcn4*<sup>+/QF</sup> × *Hcn4*<sup>+/QF</sup> crosses (10 *Hcn4*<sup>+/+</sup>, 18 *Hcn4*<sup>+/QF</sup>, and 0 *Hcn4*<sup>QF/QF</sup> pups), suggesting that HCN4 containing WT M407/Y409 is required for development. However, heterozygous *Hcn4* mutant mice (*Hcn4*<sup>+/QF</sup>) were viable and born in ~1:1 proportion to WT littermates from *Hcn4*<sup>+/QF</sup> × *Hcn4*<sup>+/+</sup> crosses (113 *Hcn4*<sup>+/+</sup> and 116 *Hcn4*<sup>+/QF</sup> pups). The  $I_f$  in SAN cells isolated from *Hcn4*<sup>+/QF</sup> mice showed reduced responses to heat compared to  $I_f$  recorded from WT littermate control SAN cells (Fig. 4a). Similar to  $I_f$  action potential rates recorded from *Hcn4*<sup>+/QF</sup> SAN cells (see Methods) had reduced  $Q_{10}$

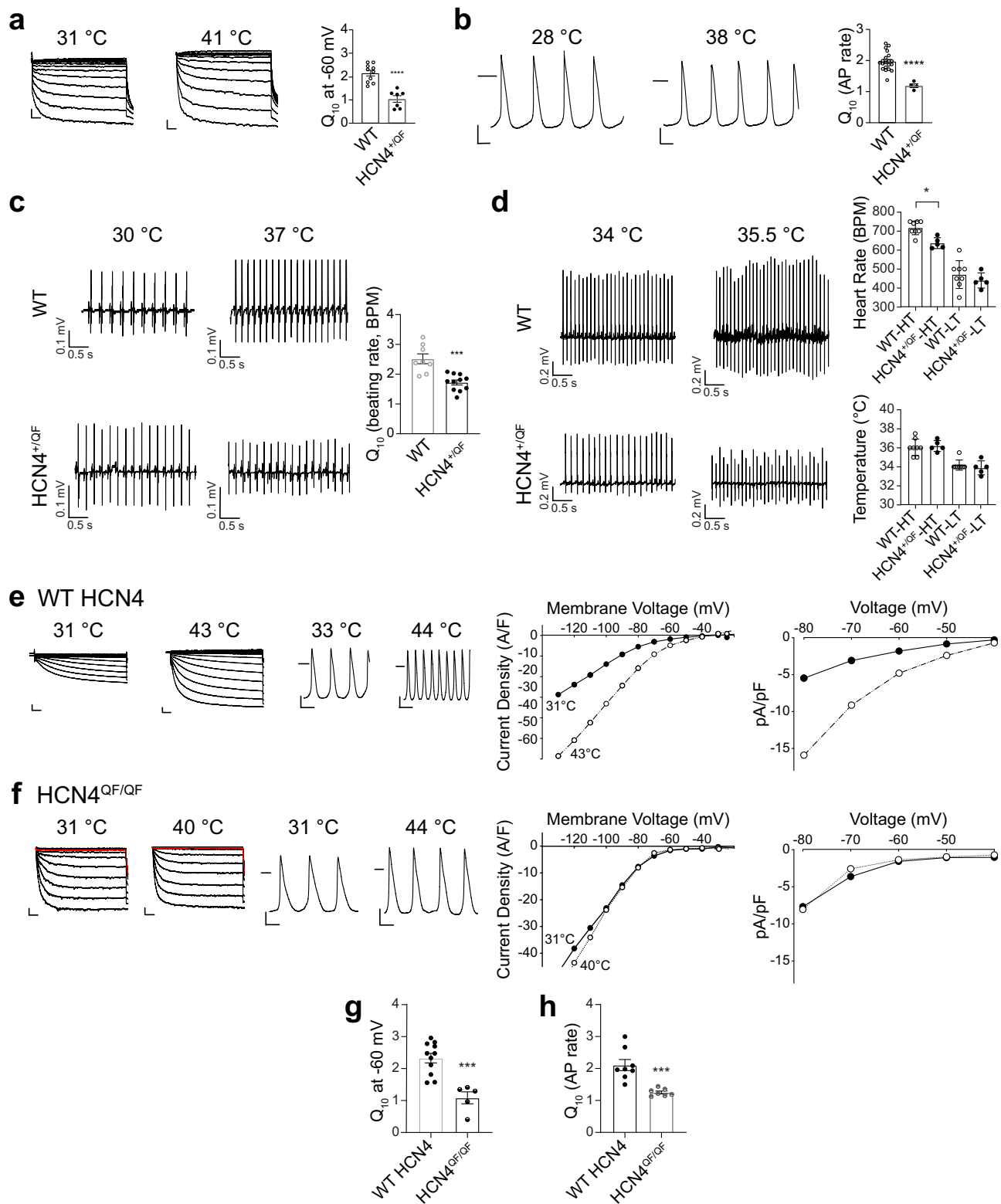


(Fig. 4b). Analysis of action potential parameters (Supplementary Fig. 7 a-h) affected by heat show action potential rate increases by heat were accompanied by more rapid ‘phase 4’ depolarization, measured as an increased diastolic depolarization rate (DDR) in WT SAN cells. The heat induced increase in DDR was abolished by the M407/Y409 mutation in  $Hcn4^{+QF}$  SAN cells (Supplementary Fig. 7c). Additionally, maximal diastolic potential (MDP) was decreased by heat in WT but not in  $Hcn4^{+QF}$  SAN cells (Supplementary Fig. 7d). These data showed key

action potential parameters associated with heart rate acceleration were responsive to heat and that these heat responses were prevented by the M407/Y409 mutation. We next recorded electrocardiograms from isolated, coronary artery perfused hearts from WT and  $Hcn4^{+QF}$  mice in order to measure heart rate (Fig. 4c). The  $Hcn4^{+QF}$  heart rates had lower  $Q_{10}$  than hearts from WT littermate controls ( $Hcn4^{+/+}$ ) (Fig. 4c and Supplementary Fig. 7i, j). Finally, we implanted telemeters for recording heart rate and body temperature in heterozygous  $Hcn4$

**Fig. 4 | Mice with *Hcn4*<sup>M407Q/Y409F</sup> mutant channels exhibit reduced rate responses to heat. **a** *I<sub>f</sub>* currents under LT (left) and HT (middle) from SAN cells of *Hcn4*<sup>+/QF</sup> mice. Bar graph: *Q*<sub>10</sub> at -60 mV from *Hcn4*<sup>+/QF</sup> (*n* = 7) and WT SAN cells (*n* = 10). Data are mean ± SEM, unpaired Student's *t*-test (two-tailed), \*\*\*\**p* < 0.0001. Scale bar: 5 pA/pF (vertical) and 500 ms (horizontal) (same for **e** and **f**). **b** AP under LT (left) and HT (middle) from *Hcn4*<sup>+/QF</sup> SAN cells. Bar graph: *Q*<sub>10</sub> on AP rates from *Hcn4*<sup>+/QF</sup> (*n* = 4) and WT SAN cells (*n* = 20), mean ± SEM, unpaired Student's *t*-test (two-tailed), \*\*\*\**p* < 0.0001. Horizontal lines mark 0 mV. Scale bars: 200 ms (horizontal) and 20 mV (vertical) (same for **e** and **f**). **c** ECG under LT (left) and HT (middle) from isolated hearts of WT (upper) or *Hcn4*<sup>+/QF</sup> (lower) mice. Bar graph: *Q*<sub>10</sub> on ECG rates (beats/min, BPM) for *Hcn4*<sup>+/QF</sup> mice (*n* = 11) and WT mice (*n* = 8). Data are mean ± SEM, unpaired Student's *t*-test (two-tailed), \*\*\**p* = 0.0002. **d** ECG under lower or increased body temperatures from unrestrained WT (upper) or *Hcn4*<sup>+/QF</sup> (lower) mice. Bar graph: in vivo heart rates (upper, *n* = 5 *Hcn4*<sup>+/QF</sup>, *n* = 8**

WT) and body temperature (lower, *n* = 5 *Hcn4*<sup>+/QF</sup>, *n* = 8 WT) used to define HT and LT. Data are mean ± SEM. \**p* = 0.048, by one-way ANOVA with Tukey's test.

**e** Representative *I<sub>f</sub>* (left) and AP (middle) under LT or HT from cultured *Hcn4*<sup>fllox/fllox</sup> SAN cells infected with Ad-mCherry-Cre and Ad-HCN4-WT. Right panels: *I<sub>f</sub>* current density-voltage relationship calculated from the same cell. The right-most panel expanded to highlight the physiological cell membrane potential range for SAN cells. **f** Similar to (**e**), *I<sub>f</sub>* and AP recordings and *I<sub>f</sub>* current density-voltage relationship from cultured *Hcn4*<sup>fllox/fllox</sup> SAN cells infected with Ad-mCherry-Cre and Ad-HCN4<sup>QF/QF</sup>. **g** *Q*<sub>10</sub> data for *I<sub>f</sub>* at -60 mV from *Hcn4*<sup>fllox/fllox</sup> SAN cells expressing HCN4 WT (*n* = 11), or HCN4<sup>QF/QF</sup> (*n* = 5). Data are mean ± SEM; unpaired Student's *t*-test (two-tailed) \*\*\**p* = 0.0003. **h** *Q*<sub>10</sub> data for AP rates from cultured *Hcn4*<sup>fllox/fllox</sup> SAN cells expressing HCN4 WT (*n* = 8), or HCN4<sup>QF/QF</sup> (*n* = 7). Data are mean ± SEM; unpaired Student's *t*-test (two-tailed), \*\*\**p* = 0.0006.

mutant *Hcn4*<sup>+/QF</sup> mice for in vivo studies. We selected 'low' and 'high' temperatures from spontaneous variations recorded over 48 h in unrestrained mice (see Methods). The *Hcn4*<sup>+/QF</sup> in vivo heart rates are lower than in vivo heart rates from WT littermate controls (*Hcn4*<sup>+/+</sup>) at normal "high" temperature (Fig. 4d). We interpreted the in vivo data to confirm the importance of HCN4 in heart rate responses to temperature. Taken together, studies in *Hcn4*<sup>+/QF</sup> mice supported a role for HCN4 coupling heat to heart rate in SAN cells, ex vivo and in vivo hearts.

To examine thermal rate responses in SAN cells that exclusively expressed the QF mutant HCN4 channels, we turned to *Hcn4*<sup>Δ2/2</sup> SAN cells<sup>20</sup> infected with Cre expressing adenovirus to develop an exchange system capable of rescuing *I<sub>f</sub>* in an *Hcn4*<sup>-/-</sup> background using cDNAs encoding WT human HCN4 or HCN4<sup>QF</sup> (see Methods). We performed voltage and current clamp studies using cultured isolated *Hcn4*<sup>-/-</sup> SAN cells expressing WT HCN4 or HCN4<sup>QF</sup>. The SAN cells rescued with WT HCN4 regained *I<sub>f</sub>* and action potential rate responsiveness to heat (Fig. 4e), similar to WT SAN cells (Figs. 1b and 2a). In contrast, the SAN cells rescued with thermally insensitive HCN4<sup>QF</sup> mutant channels failed to increase *I<sub>f</sub>* or action potential rate (Fig. 4f) in response to heat. The *Q*<sub>10</sub> values for *I<sub>f</sub>* (Fig. 4g) and SAN action potential rate (Fig. 4h) after rescue with WT HCN4 were ~2.0. Taken together, these data from CRISPR/Cas9 gene edited mice and SAN cells with *Hcn4* excision and rescue with WT HCN4 or HCN4<sup>QF</sup> channels showed that M407/Y409 were required for heat responses for SAN action potentials and *I<sub>f</sub>* and that an ion channel with a modest *Q*<sub>10</sub> (i.e. ~2) can operate a fundamental biological response to heat.

### HCN4 thermal sensing is independent of the cyclic nucleotide binding domain

HCN4 belongs to a family of ion channel proteins that are endowed with and named for a cyclic nucleotide binding domain<sup>25</sup>. Heart rate accelerates as part of the 'fight or flight' physiological response due to increased intracellular cAMP that activates HCN4 through the cyclic nucleotide binding domain, causing increased *I<sub>f</sub>* and accelerated action potential initiation<sup>26</sup>. Indeed, SAN *I<sub>f</sub>* increased upon exposure to isoproterenol, a β adrenergic receptor agonist<sup>19,27</sup>, as did the current recorded from HEK cells expressing HCN4 and dialyzed with cAMP (Fig. 5a, left panels). Dialysis of cAMP into HEK cells shifted the half maximal activation of the HCN4 current to more depolarized cell membrane potentials (Fig. 5a, right panels), an effect similar to that of heat-induced activation of HCN4 (Fig. 3g). Furthermore, cAMP and heat both hastened the activation kinetics (Figs. 2 and 5), suggesting that these signals may operate on HCN4 to increase the current through a shared mechanism. Based on this observation, we next generated a validated loss of function mutation (EA mutant, containing R669E and T670A) in the *HCN4* cyclic nucleotide-binding domain<sup>13</sup>. The EA mutant HCN4 channels failed to increase HCN4 current (Fig. 5b, left panels) or affect the half maximal activation voltage (Fig. 5b, right panels) upon cAMP exposure. However, EA mutant channels were

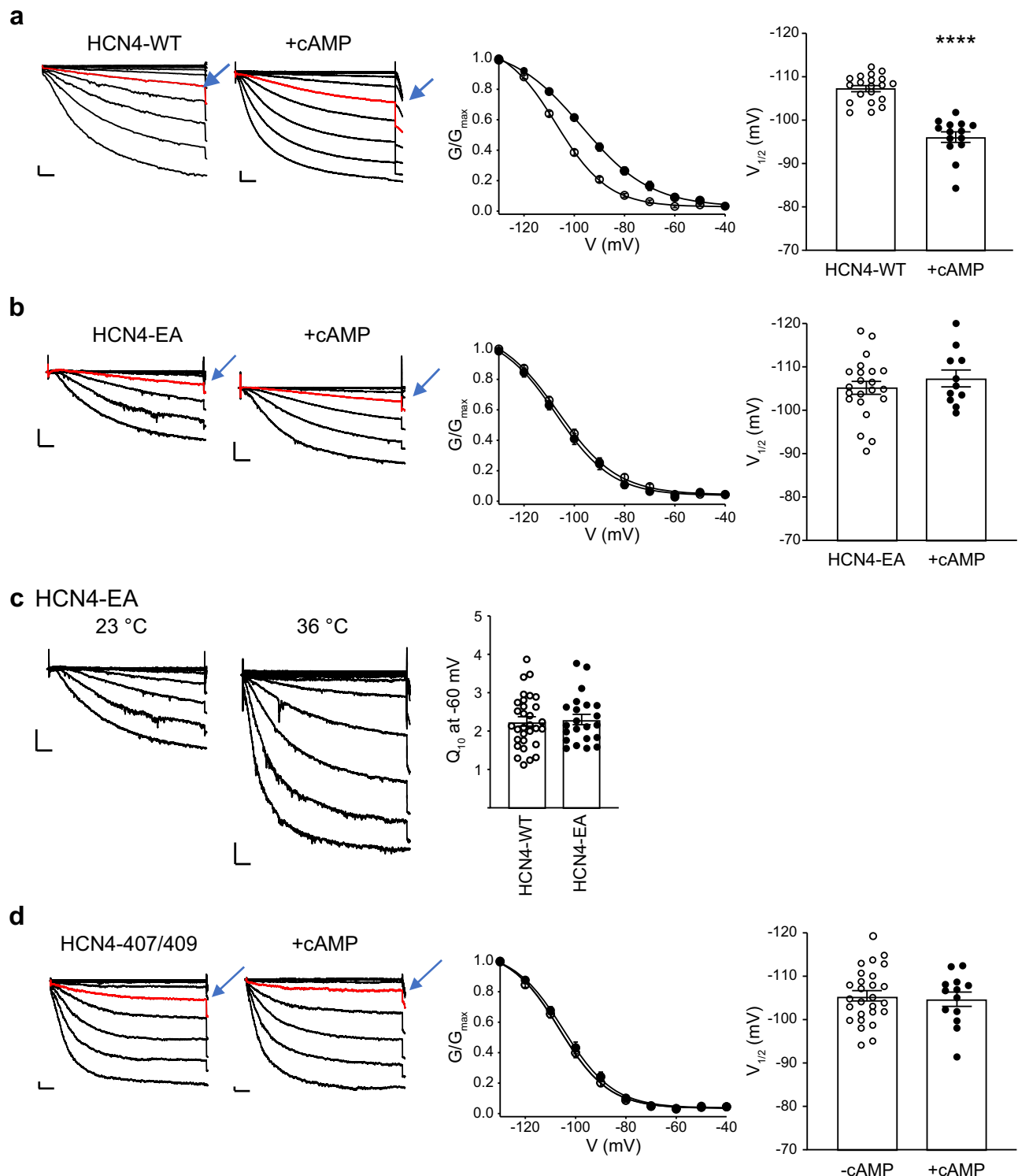
responsive to increases in temperature, showing elevated steady-state current and faster activation. *Q*<sub>10</sub> was not different from wildtype channels (Fig. 5c). We considered the possibility that temperature increases augmented HCN4 current by increasing cAMP. However, we did not detect an increase in cAMP in SAN cells or HEK 293 cells after heat exposure (Supplementary Fig. 8). We next asked if cAMP responses required the M407/Y409 motif; HCN4 current recorded from M407Q/Y409F mutants was unresponsive to cAMP (Fig. 5d, Supplementary Table 2). Collectively, we interpret these findings to show that HCN4 ion channels require M407/Y409 to respond to heat and cAMP.

### Discussion

The activity of all ion channels and of proteins in general is affected by change in temperature, because it affects their internal motion<sup>28</sup>. However, only very few channels have a temperature coefficient (*Q*<sub>10</sub>) >2 and are thus considered temperature dependent, such as members of the TRP and K2P families of channels<sup>29</sup>. In the case of HCN4, we have quantified here a *Q*<sub>10</sub> of 2, that is borderline with the definition of thermosensor. However, this is not surprising given the crucial role of this channel in controlling heart rate. Indeed, stability of heart rate is essential and even a tiny change in open probability of the channel can alter it. A clear example of this is the extremely low single channel conductance of HCN (1 pS<sup>30,31</sup>), clearly related to the need of fine tuning their response to extra and intracellular stimuli for the sake of stability.

The HCN family of ion channels are defined by a characteristic voltage activated inward current and a cyclic nucleotide response element. Our most complete understanding of the impact of the cAMP response amongst HCN family channels involves the role of HCN4 in heart rate acceleration, a cornerstone of the fight or flight stress response. Up until now, cAMP responses were thought to be the sole mechanism for augmenting HCN channel currents for physiological purposes, including the canonical case of *I<sub>f</sub>* underpinning heart rate acceleration. Our findings add a core concept in cardiac physiology by showing in mice that HCN4 is also responsible for heat triggered increases in heart rate, a feature of all vertebrates<sup>32</sup>. The finding that HCN4 heat sensing relies on two key amino acids of one intracellular linker domain is in line with a recent evidence that Shaker-IR potassium channel also depends upon a homologous intracellular linker domain for thermal responses<sup>33</sup>. This raises the question whether the (4-5) linker contributes to a general mechanism for heat sensing in ion channels. Although our study has focused on the role of HCN4 in accelerating heart rate, we found that the other HCN family members (HCN1 and HCN2) share the critical M407/Y409 residues, albeit with differences in numbering. We found that HCN1 and 2, in addition to HCN4, use the same, concise heat sensing mechanism for augmenting ionic currents. HCN1 and 2 are widely expressed in brain<sup>34</sup>, including in regions known to participate in thermal sensing and response. Thus, our work supports future studies to determine if HCN channels contribute more broadly to the systems biology of heat.





The major isoform underlying  $I_f$  in sinoatrial cells is undoubtedly HCN4. Based on various knockout models, HCN4 is responsible for about 75 % of the current in SAN cells<sup>35–37</sup>. The rest of  $I_f$  is mainly provided by HCN1 and, to a lesser extent, HCN2 channels<sup>38,39</sup>. These findings are also consistent with studies on the expression level of the three isoforms in the sinoatrial node<sup>40</sup>. Thus, our data suggest that the effect of heat on the HCN1 and HCN2 isoforms is not strong enough to increase  $I_f$  in a manner relevant to increasing heart rate. Another possibility is that M407/Y409-mutated HCN4 channels form heteromers with HCN1 or HCN2, thereby impairing the heat sensitivity of these isoforms.

Our studies present evidence that heat sensing is a dominant, but previously unanticipated, mechanism central to the regulation of HCN channels. Loss of M407/Y409 residues, in M407Q/Y409F mutants, prevented heat and cAMP responses. In contrast, a well described loss of function mutation in the cyclic nucleotide binding domain (EA)<sup>13</sup> disabled cAMP responses without affecting heat triggered  $I_f$  enhancement or action potential acceleration. Thus, cAMP responses are dispensable to heat responses while the M407/Y409 heat response motif is required for both heat sensing and cAMP responses. Further, our experiments show that increases in cAMP are not required for heat-induced increases in  $I_f$ . Notable, also, is our finding that SAN cells



**Fig. 5 | Heat sensing is required for cAMP-dependent activation of HCN4.**

**a** Representative  $I_f$  currents recorded from *HCN4* transfected HEK 293 cells with or without intracellular dialysis of cAMP (1 mM) (left panel). Red traces indicated current amplitude at -90 mV for comparison. Boltzmann distribution for *HCN4* transfected HEK 293 cells (middle panel) and summary data for midpoint voltage of activation (right panel,  $V_{1/2}$ ). Data are presented as mean values  $\pm$  SEM. Unpaired Student's *t*-test (two-tailed), \*\*\*\* $p < 0.0001$ ,  $n = 20$ , HCN4-WT,  $n = 14$  HCN4-WT + cAMP. **b** Representative  $I_f$  currents recorded from mutant *HCN4* (EA) transfected HEK 293 cells with or without intracellular dialysis of cAMP (1 mM) (left panel). Red traces indicated current amplitude at -100 mV for comparison. Data are analyzed and displayed in **(b)** middle and right panels as in **(a)** panel (above). Data are presented as mean values  $\pm$  SEM.  $n = 22$  HCN4-EA,  $n = 11$  +cAMP. **c** Representative  $I_f$  currents recorded under lower (left) and increased (middle) temperature

conditions from cultured HEK 293 cells expressing *HCN4* EA mutants. Summary  $Q_{10}$  data for  $I_f$  currents at -60 mV from HEK 293 cells (right panel). Data are presented as mean values  $\pm$  SEM,  $n = 31$  HCN4-WT,  $n = 22$  HCN4-EA. Example tracings and summary data are calculated using data from the same cell. **d** Representative  $I_f$  currents in the presence or absence of intracellular dialysis with cAMP (1 mM) (left panels) in *HCN4*<sup>407/409</sup> mutant expressing HEK 293 cells. Red traces indicated current amplitude at -90 mV for comparison. Right two panels, *HCN4*<sup>407/409</sup> current activation curves without (empty symbols) and with cAMP (1 mM) (filled symbols) dialysis. Summary data for midpoint voltage of activation ( $V_{1/2}$ ) with ( $n = 13$ ) or without cAMP ( $n = 27$ ) (right). Data are presented as mean values  $\pm$  SEM. Solid lines show Boltzmann fitting to the data (middle, see Methods). Values are reported in Supplementary Table 2. **a–d** Scale bars are 500 ms horizontal and 5 pA/pF vertical.

are resistant to heat-induced rate increases after exposure to  $I_f$  antagonists, yet sustain a normal rate increase to isoproterenol (i.e., an agonist operating the cAMP pathway) in the presence of these antagonists (Supplementary Fig. 2a). We interpret these findings to suggest that if heat-induced increases in cAMP transpire in native cells that they are likely modest and considerably lower than cAMP increases induced by  $\beta$ -adrenergic receptor agonist activation. Taken together, these findings strongly suggest that heat actions on HCN4 are independent of the cAMP pathway.

The lethality of the homozygous M407/Y409 mutation may be due to its lack of response to cAMP. In agreement with this concept, homozygous mice with a point mutation in the CNBD (HCN4 R669Q), which abolishes cAMP binding, also die during embryonic development<sup>35</sup>. Based on these findings we suspect that cAMP-dependent activation of HCN4 is required for proper development.

In homeothermic organisms core body temperature increases with exercise<sup>41,42</sup> and fever<sup>43</sup>, both conditions of augmented adrenergic tone. Thus, our findings reveal a mechanistic parsimony showing that HCN4, a channel that contributes to a highly conserved fight or flight heart rate increase, is configured to respond to heat and cAMP. Our findings suggest that heat sensing is core to canonical HCN responses to heat and cyclic nucleotide activation and that the two signals converge to a common molecular mechanism, i.e the unfolding of the S4-S5 linker helix. It will be interesting to learn if HCN channels distributed in brain regions important for systemic thermal control contribute to physiological or disease processes related to increased core body temperature.

## Methods

### Ethical statement

All experiments involved using animals were carried out in accordance with the guidelines and policies of Institutional Animal Care and Use Committee of Johns Hopkins University, with approval numbers MO17M290 and MO20M274.

### A general note about experiment temperatures

Our experimental design rigorously adheres to the principle of internal consistency, ensuring that temperature comparisons are made within the same experimental sample—be it a cell, heart, or mouse. This approach underpins our data presentation, where the distinction between low and high temperature conditions is derived from within-sample changes rather than cross-sample comparisons.

In detailing our experimental conditions across various settings—ranging from HEK cell cultures, isolated or cultured sinoatrial node cells, to isolated hearts and live mice experiments—it's important to emphasize the context-specific nature of our temperature definitions. For HEK 293 cells, the low temperature (LT) was set at the lower 20 °C range, aligning with common practices in HCN channel current studies to facilitate comparison with existing literature. For sinoatrial node cells, the LT was adjusted to the lower 30 °C to ensure the preservation of spontaneous cellular activity, a principle also applied to isolated

heart experiments. The in vivo LT and HT were selected from spontaneous variation in the core body temperatures over a 48 h interval in free living mice housed at  $22 \pm 1$  °C (45% to 50% humidity, with lights set to a 12 h light/dark cycle) and implanted with ECG and temperature monitors. Additionally, certain cellular studies explored HT conditions, around 40 °C, to mimic fever scenarios in animals or humans, thereby encompassing a broad physiological relevance.

### SAN cell isolation, culture and infection

Method of isolation of SAN cells from mice was modified and performed according to previously published methods<sup>27</sup>. Mice were anesthetized with avertin (20  $\mu$ l/g, i.p.) and heparinized (8000 U/kg, i.p.), and monitored until unresponsive. The heart was excised and placed into ice-cold Tyrode's solution, consisting of (mM): 140.0 NaCl, 5.0 HEPES, 5.5 Glucose, 5.4 KCl, 1.8 CaCl<sub>2</sub>, and 1.0 MgCl<sub>2</sub>. The pH was adjusted to 7.4 with NaOH. After aortic cannula, the heart was perfused by Ca<sup>2+</sup>-free Tyrode's solution first, then followed by digestion solution contain collagenase type II (Worthington) and protease type XIV (Sigma). The SAN region, delimited by the crista terminalis, atrial septum and orifice of superior vena cava, was dissected free from the heart and was cut into smaller pieces. SAN tissue pieces were digested in 5 ml of solution containing collagenase type I, elastase (Worthington), and protease type XIV (Sigma) for 20–30 min. The tissue was transferred to 10 ml of Kraft-Bruhe medium containing (mM): 100.0 potassium glutamate, 5.0 HEPES, 20.0 Glucose, 25.0 KCl, 10.0 potassium aspartate, 2.0 MgSO<sub>4</sub>, 10.0 KH<sub>2</sub>PO<sub>4</sub>, 20.0 taurine, 5.0 creatine, 0.5 EGTA, and 1.0 mg/ml BSA, with pH adjusted to 7.2 using KOH. The tissue was agitated using a glass pipette for 10 min. The cells were either kept at room temperature and studied within 7 h, or used for culture studies.

Freshly isolated SAN cells were put into 35 mm tissue culture plates with Media 199 containing Blebbistatin 10 mM (ApexBio B1387-10), 5% FBS, Primocin (Invivogen) and ITS. Fresh medium containing Ad-mCherry-Cre (Vector Biolabs 1773), Ad-HCN4-wt or Ad-HCN4-407/409 was added to the plates at a multiplicity of infection of 100.

### HEK 293 cell culture and transfection

HEK 293FT cells were cultured in DEME (ThermoFisher Scientific, catalog #11995) containing 10% FBS, NEAA (ThermoFisher Scientific, catalog #11140050) and GlutaMax (ThermoFisher Scientific, catalog #35050079). For transfection, cells were seeded between 250,000 to 300,000 cells per 35 mm dish the day before transfection and were then co-transfected with 0.8  $\mu$ g of an *HCN* plasmid and 0.5  $\mu$ g of an eGFP plasmid to aid in identifying transfected cells. We used jetPRIME reagent (Polyplus) for transfection.

### cAMP level measurement

SAN cells isolated from 2 mice by the method described above were combined to increase cell number for cAMP assay. All the groups (room temperature controls and high temperature testing groups) were treated with IBMX 100  $\mu$ M for 10 min at room temperature ( $23 \pm 1$  °C) before subjecting no further treatment (control), ISO 1  $\mu$ M

10 min at room temperature as a positive control or incubate in warmer bath at  $38 \pm 1$  °C for 10 min.

HEK 293 cells were suspended in Tyrode's solution containing 500  $\mu$ M IBMX and 0.1% BSA. Subsequently, cells were treated for 30 min in this buffer with DMSO at room temperature (control), 25  $\mu$ M forskolin at room temperature (positive control), or DMSO at  $38 \pm 1$  °C.

The cAMP level was measured by using LANCE Ultra cAMP Detection Kit ((TRF0262) Revvity, MA, USA). The final data were normalized by cell numbers in each group.

### Cellular electrophysiology and temperature control

SAN cells or HEK 293FT cells transfected with human HCN4 WT or mutant plasmids were placed in temperature-controlled chamber of around 1 ml volume of Tyrode's solution at room temperature (around  $23 \pm 1$  °C) or warmer temperatures as indicated. Temperature control was performed by TC-344B Dual Channel Automatic Temperature Controller (Warner Instruments, Holliston, MA 01746, USA) used with both a heated chamber and solution in-line heater to rapidly change or maintain a desired temperature. SAN cells with the characteristic morphology (spindle or spider shape) and spontaneous activity were studied. Adenovirus infected SAN cells were identified by mCherry expression. SAN cells were also identified electrophysiologically by typical spontaneous action potentials with slow depolarizing phase 4 and the  $I_f$  currents in electrophysiological experiments. HEK 293FT cells with HCN4 plasmids transfection were identified by GFP expression.

Spontaneous action potentials and  $I_f$  currents were recorded using the perforated (amphotericin B or  $\beta$ -escin) patch-clamp technique on single SAN cell at various temperatures as indicated in Tyrode's solution. Temperature was recorded using Digidata 1440 A (Molecular Device, San Jose, CA 95134, USA) and pClamp 11 (Molecular Device). The patch pipette was filled with (mM): 130.0 potassium aspartate, 10.0 NaCl, 10.0 HEPES, 0.04 CaCl<sub>2</sub>, amphotericin B 240  $\mu$ g/ml with pH adjusted to 7.2 with KOH.  $\beta$ -escin 50  $\mu$ M was substituted for amphotericin B to allow dialysis of cAMP or PKI. For recording HCN channels currents in HEK 293FT cells, bath solution composed with (mM): 110.0 NaCl, 0.5 MgCl<sub>2</sub>, 1.8 CaCl<sub>2</sub>, 30.0 KCl, 5.0 HEPES, pH adjusted to 7.4 with NaOH; intracellular solution contains (mM): 130.0 KCl, 10.0 NaCl, 0.5 MgCl<sub>2</sub>, 1.0 EGTA, 5.0 HEPES, pH adjusted to 7.4 with KOH. Data were acquired at 100 kHz using Axopatch 200B (Molecular Device). When recording  $I_f$  currents or HCN4 channels currents, membrane potential was held at -40 mV, the voltage steps were applied for 5 s ranging from -130 mV – -20 mV in 10 mV increments or vice versa.

### HCN channel current and tail current analysis

The impact of temperature on  $I_f$  or HCN current activation was obtained from tail current analysis. The latter were obtained from a two-step voltage clamp protocol: SAN cells or HEK293 cells were first stepped for 5 s to conditioning voltages between -40 and -130 mV before clamping to a common voltage at -130 mV, where tail currents were collected and expressed as current density (pA/pF).

Activation curves were obtained by plotting tail currents as absolute values or after normalization between zero (channels closed) and one (channels maximally open) as a function of conditioning voltages. Data were fitted with the Boltzmann equation:

$$G = G_{\max} / [1 + \exp((V - V_{1/2})/k)] + A, \quad (1)$$

where  $G_{\max}$  is the maximal conductance,  $V_{1/2}$  the half-activation voltage,  $A$  is a conductance offset and  $k$  the inverse-slope factor =  $RT/zF$  (all in mV). For normalization of activation curves the ratio  $G/G_{\max}$  was calculated and  $G_{\max}$  in Eq. 1 was set to 1.

The time constant of activation was determined by mono-exponential function fitting the current evoked during hyperpolarizing voltage pulse to -130 mV, the initial lag in the activation of HCN channel currents was excluded from the fitting procedure.

### Ex vivo Langendorff-perfused heart rate measurements

ECG recording from Langendorff-perfused hearts was performed as following: Briefly, excised hearts were rapidly mounted on a Langendorff apparatus (ADInstruments Inc. Colorado Springs, USA) for retrograde aortic perfusion at a constant flow of 4 ml/min with oxygenated (95% O<sub>2</sub>, 5% CO<sub>2</sub>) Krebs-Henseleit solution consisting of (mM): 25.0 NaHCO<sub>3</sub>, 118.0 NaCl, 4.7 KCl, 1.2 MgSO<sub>4</sub>, 1.2 KH<sub>2</sub>PO<sub>4</sub>, 2.5 CaCl<sub>2</sub>, and 11.0 Glucose, with pH equilibrated to 7.4. Each perfused heart was immersed in a water-jacketed bath and the bath temperature was monitored by T-type Implantable Thermocouple Probe (IT-21) (ADInstruments Inc.). ECG measurements from the intact heart were continuously recorded with Isolated Heart MAP Electrode Set (Mouse, ADI) (ADInstruments Inc.). After the heart was allowed to stabilize for at least 20 min, the heart rate and bath temperature were recorded by Powerlab (ADInstruments Inc.), bath temperature was controlled or changed by circulating water from bath heater and circulator.

### Telemetry ECG and body core temperature recording

Surgical implantation of ECG and body core temperature-sensing and recording telemeters was conducted as described<sup>44</sup>. Mice were allowed to recover for at least 7 days prior to experiments.

### Cloning and mutagenesis

The plasmid (pENTR223.1-HCN4) containing the human HCN4 cDNA (HsCD00350637) was ordered from DNASU Plasmid Repository (<http://dnasu.org/DNASU/GetCloneDetail.do?cloneid=350637>). The HCN4 cDNA was cloned into the CVM promoter containing expression vector pcDNA6.2-V5-DEST by Gateway cloning (ThermoFisher Scientific). Human HCN1 (NM\_021072.4) and HCN2 (NM\_001194.4) cDNAs were synthesized by TWIST Bioscience and cloned into the pTwist-CMV-BetaGlobin-WPRE-Neo mammalian expression vector. Single and double mutations targeting the candidate residues identified by computational modeling were generated by the Q5 Site-directed mutagenesis kit (New England BioLabs). More complex compound mutations were generated in synthetic gene fragments (TWIST Bioscience), which were then used to replace the corresponding regions in the wildtype plasmids with NEBuilder® HiFi DNA Assembly Cloning Kit (New England BioLabs). All plasmids were fully sequenced. The rabbit M408Q/Y410F (corresponding to M407Q/Y409F on mouse and human HCN4) were generated by the Q5 Site-directed mutagenesis kit.

### HCN4 computational modeling

The transmembrane portion of the open and cAMP-activated structures of HCN4 overlapped using the program MOE (Molecular Operating Environment). The residue substitutions to be studied were modeled in the human structures with the same molecular modeling program. The apolar and polar solvent exposed areas of each atom in the human structures were calculated using a Shrake-Rupley algorithm with a probe radius of 1.4 Å using computational routines provided by Bio.PDB (v 1.79), pandas (v 1.4.1), and Numpy (v 1.22.2) python (v 3.8) modules, summed total for all, main-chain, and side-chain atoms, as well as separated contributions of their polar and apolar areas. The theoretical contributions to the  $\Delta$ cp of hydration per unit of SASA were calculated using interpolated values at 37 °C from Table 7 of reference<sup>45</sup>. The linear interpolation used the reported values at 25 °C and 50 °C. The python Jupyter notebook developed and auxiliary files are available in the GitHub repository ([https://github.com/mabianchet/HCN4\\_SASA](https://github.com/mabianchet/HCN4_SASA)).

### M407Q/Y409F knock in mice

*Hcn4*-M407Q/Y409F-knockin mice were generated on a C57BL/6J background using the CRISPR/Cas9 technology at the Johns Hopkins Transgenic Core. A CRISPR guide RNA (Alt-R® CRISPR-Cas9 crRNA, IDT), sequence: 5'- taggtcatgtggaagatctg-3', was designed to target

mouse *Hcn4*. A synthetic ssODN for homology-directed repair was designed to harbor missense mutations for M407Q (ATG→caG), Y409F (TAT→Ttc), and silent mutations encoding I404 (ATC→ATt) and F405 (TTC→TTt) to create an HphI restriction site for genotyping. The sequence of the ssODN was 5'-CAATGAGGTTCACGATGCGTAC-CACGGCGCTGGCCAGGTCgaAGGTCTgGTGaAAaATCTGTGGAGTCGA GCCATGGCACAGACAAGTAAGCGGTC-3'. Genotyping of founder mice, and subsequent offspring was performed by first PCR amplifying a 385 bp fragment from tail DNA with a pair of primers (HCN4QF\_Fwd: GTGTTGCCATGGTGCCCTCCAG and HCN4QF\_Rev: TGCCACCTGCT GGGATTCAGGA). Then, both Sanger sequencing and HphI digestion of the PCR amplified fragments were used for genotyping. 28 out of 43 F0 mice were targeted by CRISPR, and 3 had correct M407Q/Y409F mutations. Two founder M407Q/Y409F mice were backcrossed with C57BL/6J mice from The Jackson Laboratory, and experiments from both lines produced similar results.

### Statistical analysis

Data are presented as mean ± SEM unless otherwise noted. Statistical analysis was performed either with one-way ANOVA or an unpaired or paired Student's *t*-test, as appropriate. Analyses were performed with Sigmaplot or Sigmastat (Systat Software, Inc. San Jose, CA 95110 USA), and Graph Pad Prism 8 (GraphPad Software, Inc. San Diego, CA 92108, USA). The null hypothesis was rejected for a *P* < 0.05.

### Movie

Movie 1 was created using the PyMOL program. The intermediate structures between the close and activated form were obtained using The Yale Morphing server (<http://www.molmovdb.org/molmovdb/morph/>; accessed May 23 2023)<sup>46</sup>.

### Reporting summary

Further information on research design is available in the Nature Portfolio Reporting Summary linked to this article.

### Data availability

The Data generated and analyzed that support the findings of this study are available from the corresponding author upon request. Additionally, the source data underlying Figs. 1f, 2a–f, 3d, 3f, g, 4a–h, 5a–d and Supplementary Fig. 1a, b, 2b, c, 3a, b, 4a, 4d–f, 5a, b, 7a–j, 8a–c are provided as a Source Data file. The source data underlying Supplementary Table 2 are provided as a separated Source Data file for Table S2. The python Jupyter notebook developed and auxiliary files are available in the Zenodo repository [<https://doi.org/10.5281/zenodo.14635261>], [<https://doi.org/10.5281/zenodo.14635412>]. Structural model of the mutants, Jupyter notebook and datasets used for the thermodynamical calculations are deposited in Zenodo [<https://doi.org/10.5281/zenodo.14635261>] and [<https://doi.org/10.5281/zenodo.14635412>]. Source data are provided with this paper.

### References

- Clark, A. J. The effect of alterations of temperature upon the functions of the isolated heart. *J. Physiol.* **54**, 275–286 (1920).
- Tanner, J. M. The relationships between the frequency of the heart, oral temperature and rectal temperature in man at rest. *J. Physiol.* **115**, 391–409 (1951).
- Kirschen, G. W., Singer, D. D., Thode, H. C. Jr. & Singer, A. J. Relationship between body temperature and heart rate in adults and children: a local and national study. *Am. J. Emerg. Med.* **38**, 929–933 (2020).
- Biel, M., Wahl-Schott, C., Michalakakis, S. & Zong, X. Hyperpolarization-activated cation channels: from genes to function. *Physiol. Rev.* **89**, 847–885 (2009).
- DiFrancesco, D. Pacemaker mechanisms in cardiac tissue. *Annu. Rev. Physiol.* **55**, 455–472 (1993).
- DiFrancesco, D. & Ojeda, C. Properties of the current if in the sinoatrial node of the rabbit compared with those of the current iK, in Purkinje fibres. *J. Physiol.* **308**, 353–367 (1980).
- Hart, G. The kinetics and temperature dependence of the pacemaker current if in sheep Purkinje fibres. *J. Physiol.* **337**, 401–416 (1983).
- Swoap, S. J. & Gutilla, M. J. Cardiovascular changes during daily torpor in the laboratory mouse. *Am. J. Physiol. Regul. Integr. Comp. Physiol.* **297**, R769–R774 (2009).
- Broman, M. E., Vincent, J.-L., Ronco, C., Hansson, F. & Bell, M. The relationship between heart rate and body temperature in critically ill patients. *Crit. Care Med.* **49**, e327–e331 (2021).
- Liu, J. et al. Heat exposure and cardiovascular health outcomes: a systematic review and meta-analysis. *Lancet Planetary Health* **6**, e484–e495 (2022).
- Voosen, P. Global temperatures in 2020 tied record highs. *Science* **371**, 334–335 (2021).
- Braunwald, E. Cardiovascular effects of climate change. *Eur. Heart J.* **45**, 3006–3008 (2024).
- Fenske, S. et al. cAMP-dependent regulation of HCN4 controls the tonic entrainment process in sinoatrial node pacemaker cells. *Nat. Commun.* **11**, 5555 (2020).
- Bolter, C. P. & Kebas, V. K. Temperature sensitivity of the human cardiac pacemaker during exercise. *Arch. Int. Physiol. Biochim.* **97**, 493–497 (1989).
- Bolter, C. P. & Atkinson, K. J. Maximum heart rate responses to exercise and isoproterenol in the trained rat. *Am. J. Physiol.* **254**, R834–R839 (1988).
- Bolter, C. P. & Atkinson, K. J. Influence of temperature and adrenergic stimulation on rat sinoatrial frequency. *Am. J. Physiol.* **254**, R840–R844 (1988).
- Thollon, C. et al. Electrophysiological effects of S 16257, a novel sino-atrial node modulator, on rabbit and guinea-pig cardiac preparations: comparison with UL-FS 49. *Br. J. Pharmacol.* **112**, 37–42 (1994).
- BoSmith, R. E., Briggs, I. & Sturgess, N. C. Inhibitory actions of ZENECA ZD7288 on whole-cell hyperpolarization activated inward current (I<sub>h</sub>) in guinea-pig dissociated sinoatrial node cells. *Br. J. Pharmacol.* **110**, 343–349 (1993).
- Wu, Y. et al. Calmodulin kinase II is required for fight or flight sinoatrial node physiology. *Proc. Natl. Acad. Sci. USA* **106**, 5972–5977 (2009).
- Stieber, J. et al. The hyperpolarization-activated channel HCN4 is required for the generation of pacemaker action potentials in the embryonic heart. *Proc. Natl. Acad. Sci. USA* **100**, 15235–15240 (2003).
- Chowdhury, S., Jarecki, B. W. & Chanda, B. A molecular framework for temperature-dependent gating of ion channels. *Cell* **158**, 1148–1158 (2014).
- Saponaro, A. et al. Gating movements and ion permeation in HCN4 pacemaker channels. *Mol. Cell* **81**, 2929–2943 e2926 (2021).
- Mistriik, P. et al. The murine HCN3 gene encodes a hyperpolarization-activated cation channel with slow kinetics and unique response to cyclic nucleotides. *J. Biol. Chem.* **280**, 27056–27061 (2005).
- Stieber, J., Stöckl, G., Herrmann, S., Hassfurth, B. & Hofmann, F. Functional expression of the human HCN3 channel. *J. Biol. Chem.* **280**, 34635–34643 (2005).
- James, Z. M. & Zagotta, W. N. Structural insights into the mechanisms of CNBD channel function. *J. Gen. Physiol.* **150**, 225–244 (2018).
- DiFrancesco, D. & Tortora, P. Direct activation of cardiac pacemaker channels by intracellular cyclic AMP. *Nature* **351**, 145–147 (1991).
- Wu, Y. et al. The mitochondrial uniporter controls fight or flight heart rate increases. *Nat. Commun.* **6**, 6081 (2015).



28. Brauchi, S., Orio, P. & Latorre, R. Clues to understanding cold sensation: thermodynamics and electrophysiological analysis of the cold receptor TRPM8. *Proc. Natl. Acad. Sci. USA* **101**, 15494–15499 (2004).
29. Lamas, J. A., Rueda-Ruzafa, L., and Herrera-Pérez, S. Ion channels and thermosensitivity: TRP, TREK, or both? *Int. J. Mol. Sci.* **20**, 2371 (2019).
30. Thon, S., Schmauder, R. & Benndorf, K. Elementary functional properties of single HCN2 channels. *Biophys. J.* **105**, 1581–1589 (2013).
31. DiFrancesco, D. Characterization of single pacemaker channels in cardiac sino-atrial node cells. *Nature* **324**, 470–473 (1986).
32. Seebacher, F. Responses to temperature variation: integration of thermoregulation and metabolism in vertebrates. *J. Exp. Biol.* **212**, 2885–2891 (2009).
33. Bassetto Jr, C. A. Z., Pinto, B., Latorre, R. & Bezanilla, F. Tuning the temperature dependence of shaker potassium channel with mutations at S4-S5 linker. *Biophys. J.* **122**, 244a (2023).
34. Combe, C. L. & Gasparini, S. Ih from synapses to networks: HCN channel functions and modulation in neurons. *Prog. Biophys. Mol. Biol.* **166**, 119–132 (2021).
35. Harzheim, D. et al. Cardiac pacemaker function of HCN4 channels in mice is confined to embryonic development and requires cyclic AMP. *EMBO J.* **27**, 692–703 (2008).
36. Hoesl, E. et al. Tamoxifen-inducible gene deletion in the cardiac conduction system. *J. Mol. Cell. Cardiol.* **45**, 62–69 (2008).
37. Baruscotti, M. et al. Deep bradycardia and heart block caused by inducible cardiac-specific knockout of the pacemaker channel gene *Hcn4*. *Proc. Natl. Acad. Sci.* **108**, 1705–1710 (2011).
38. Fenske, S. et al. Sick sinus syndrome in HCN1-deficient mice. *Circulation* **128**, 2585–2594 (2013).
39. Ludwig, A. et al. Absence epilepsy and sinus dysrhythmia in mice lacking the pacemaker channel HCN2. *EMBO J.* **22**, 216–224 (2003).
40. Herrmann, S., Layh, B. & Ludwig, A. Novel insights into the distribution of cardiac HCN channels: an expression study in the mouse heart. *J. Mol. Cell. Cardiol.* **51**, 997–1006 (2011).
41. Wendt, D. L., Van Loon, L. J. C. & Van Marken Lichtenbelt, W. D. Thermoregulation during exercise in the heat. *Sports Med.* **37**, 669–682 (2007).
42. Kenny, G. P. & McGinn, R. Restoration of thermoregulation after exercise. *J. Appl. Physiol.* **122**, 933–944 (2017).
43. Nakamura, K. Central circuitries for body temperature regulation and fever. *Am. J. Physiol. Regul. Integr. Comp. Physiol.* **301**, R1207–R1228 (2011).
44. Wu, Y., Valdivia, H. H., Wehrens, X. H. T. & Anderson, M. E. A single protein kinase A or calmodulin kinase II site does not control the cardiac pacemaker Ca<sup>2+</sup> clock. *Circ. Arrhythm. Electrophysiol.* **9**, e003180 (2016).
45. Makhatadze, G. I. & Privalov, P. L. Heat capacity of proteins: I. Partial molar heat capacity of individual amino acid residues in aqueous solution: hydration effect. *J. Mol. Biol.* **213**, 375–384 (1990).
46. Krebs, W. G. & Gerstein, M. SURVEY AND SUMMARY: the morph server: a standardized system for analyzing and visualizing macromolecular motions in a database framework. *Nucleic Acids Res.* **28**, 1665–1675 (2000).

## Acknowledgements

We appreciate review and suggestions to a draft manuscript by Dr. Francisco Bezanilla of University of Chicago. Prof. Dr. Gerhard Thiel of The Technical University of Darmstadt provided critical review and suggestions to the revision of manuscript. Ms. Pauline Phi-Han Nguyen for her graphic artist help. This work was funded in part by the National Institutes of Health R35HL140034 (to MEA), Fondation Leducq grant TNE 19CV03 (to AM), Glenn Foundation for Medical Research and AFAR Research Grant for Junior Faculty, Karen and Ethan Leder CIM Human

Aging Project, the Johns Hopkins Older Americans Independence Center Research Education Core grant P30AG021334 (PI Jeremy Walston), the Johns Hopkins Center For AIDS Research Faculty Development Grant P30AI094189 (PI Richard Chaisson) (to QW). National Institutes of Health R01GM114250, 9th Annual Discovery fund in honor of Dr. Michel Mirowski and his wife Anna for Cardiovascular Research, and Melanoma Research Alliance award 90099653 (Chaim Weizman Fund) (to MB). American Heart Association Predoctoral Fellowship 905878 (to OERG).

## Author contributions

Y.W. and M.E.A. conceptualized the study, interpreted the data and wrote the manuscript with the input of co-authors. Y.W. designed and performed all electrophysiological experiments (ion channel and action potential), isolated heart and in vivo experiments, analyze the data. Q.W. generated QF mice and most of the experimental reagents, contributed significantly to writing and revising the manuscript. J.G. assisted in vivo experiments and generated reagents. G.L.-C. assisted cAMP experiments and analyzed data. M.B. conducted computational modeling and in silico thermodynamical analysis, data interpretation and helped revise the manuscript. A.L. provided HCN4<sup>tm1</sup> mice and provided substantial input in editing the manuscript. A.M. provided the rbHCN4 construct and provided critical input to multiple drafts of the manuscript, and contributed significantly to revising the manuscript. O.R.G. generated experimental reagents. E.N.A. generated graphical depictions of HCN4.

## Competing interests

The authors declare no competing interests.

## Additional information

**Supplementary information** The online version contains supplementary material available at <https://doi.org/10.1038/s41467-025-57358-9>.

**Correspondence** and requests for materials should be addressed to Yuejin Wu or Mark E. Anderson.

**Peer review information** *Nature Communications* thanks Leandro Zuñiga and the other, anonymous, reviewer(s) for their contribution to the peer review of this work. A peer review file is available.

**Reprints and permissions information** is available at <http://www.nature.com/reprints>

**Publisher's note** Springer Nature remains neutral with regard to jurisdictional claims in published maps and institutional affiliations.

**Open Access** This article is licensed under a Creative Commons Attribution-NonCommercial-NoDerivatives 4.0 International License, which permits any non-commercial use, sharing, distribution and reproduction in any medium or format, as long as you give appropriate credit to the original author(s) and the source, provide a link to the Creative Commons licence, and indicate if you modified the licensed material. You do not have permission under this licence to share adapted material derived from this article or parts of it. The images or other third party material in this article are included in the article's Creative Commons licence, unless indicated otherwise in a credit line to the material. If material is not included in the article's Creative Commons licence and your intended use is not permitted by statutory regulation or exceeds the permitted use, you will need to obtain permission directly from the copyright holder. To view a copy of this licence, visit <http://creativecommons.org/licenses/by-nc-nd/4.0/>.

© The Author(s) 2025